Aberrant fatty acid metabolism in skeletal muscle contributes to insulin resistance in zinc transporter 7 (*znt7*)-knockout mice

Liping Huang[‡§¶1], Surapun Tepaamorndech[¶‖], Catherine P. Kirschke[‡], John W. Newman[‡§], William R. Keyes[‡], Theresa L. Pedersen[‡2], and Jureeporn Dumnil[‖]

From the ‡Obesity and Metabolism Research Unit, United States Department of Agriculture/Agricultural Research Service/Western Human Nutrition Research Center, Davis, California 95616, §Department of Nutrition and ¶Integrative Genetics and Genomics Graduate Group, University of California, Davis, California 95616, and ‖Food Biotechnology Research Unit, National Center for Genetic Engineering and Biotechnology (BIOTEC), 113 Thailand Science Park, Phahonyothin Road, Pathum Thani 12120, Thailand

Edited by Jeffrey E. Pessin

ZnT7 (Slc30a7) is a widely expressed zinc transporter involved in sequestration of zinc into the Golgi apparatus and vesicular compartments. *znt7*-knockout (KO) mice are mildly zinc-deficient and lean. Despite their lean phenotype, adult male *znt7*-KO mice are prone to insulin resistance. We hypothesized that fat partitioning from adipose to nonadipose tissues causes insulin resistance in *znt7*-KO mice. Here, we used biological and biochemical methods, including fatty acid and oxylipin profiling, EM, immunohistochemistry, quantitative RT-PCR, and Western blot analysis, to identify the underlying mechanism of insulin resistance in *znt7*-KO mice. We found that insulin resistance in this model was primarily associated with increased intracellular fatty acid levels in the skeletal muscle, which promoted intracellular lipid accumulation and production of bioactive lipid mediators, such as 12,13-dihydroxyoctadecanoic acid (12,13-DiHOME) and 12-hydroxyeicosatetraenoic acid (12-HETE). The expression of fatty acid–binding protein 3 (Fabp3) was dramatically up-regulated in the *znt7*-KO muscle cells accompanied by increased expression of Cd36, Slc27a1, and Slc27a4, the three major fatty acid transporters in the skeletal muscle. We also demonstrated that *znt7*-KO muscle cells had increased fatty acid oxidative capacity, indicated by enlarged mitochondria and increased mRNA or protein expression of key enzymes involved in the fatty acid mitochondrial shuttle and β-oxidation. We conclude that increased fatty acid uptake in the *znt7*-KO skeletal muscle is a key factor that contributes to the excessive intracellular lipid deposit and elevated production of bioactive lipid mediators. These mediators may play pivotal roles in oxidative stress and inflammation, leading to insulin resistance.

Cellular zinc homeostasis is tightly regulated through two families of zinc transporters (Slc30a and Slc39a)[3] (1, 2) and other small proteins, such as metallothioneins (3). In general, Slc30a family members (Slc30a1–10) are involved in sequestration of zinc into intracellular compartments or export of zinc out of the cell when cellular zinc is in excess. In contrast, Slc39a family members (Slc39a1–14) play roles in either zinc uptake from the extracellular space or zinc release from the intracellular stores into the cytoplasm when cellular zinc concentration is low (1, 2). The expression of zinc transporters can be ubiquitous or tissue- or cell-specific. For example, Slc30a1 is expressed ubiquitously, whereas Slc30a8 is abundantly and almost exclusively expressed in the pancreatic islet. Between the two extremes, expression of many other zinc transporters can be widespread at various levels. For example, ZnT7 is ubiquitously expressed among tissues/cell types; however, the expression level differs greatly. As a result, the impact of a null mutation in an Slc30a or Slc39a gene on zinc metabolism varies due to differences in expression levels in the body.

We reported previously that ZnT7 was expressed in mouse skeletal muscle (4), adipose tissue (5), β-cells in the islet of the pancreas (6), epithelium of the small intestine (7), and prostate (8). Consequently, the *znt7*-knockout (KO) mouse displays phenotypes that are closely associated with its protein expression level in a given tissue or cell type (9). A reduced capability of maintaining cellular zinc level at a normal range contributes to zinc deficiency in *znt7*-KO mice, which results from decreased dietary zinc absorption in the gut and consequently reduced zinc accumulation in organs, such as the bone, liver, and kidney (10). We have also demonstrated that male adult

[1] To whom correspondence should be addressed: Obesity and Metabolism Research Unit, USDA/ARS/Western Human Nutrition Research Center, 430 West Health Sciences Dr., Davis, CA 95616. Tel.: 530-754-5756; Fax: 530-752-5271; E-mail: liping.huang@ars.usda.gov.
[2] Present address: Advanced Analytics, 1718 Amador Way, Woodland, CA 95695.

[3] The abbreviations used are: Slc, solute carrier; *znt7*, zinc transporter 7; *Cd36*, cluster of differentiation 36; *Slc27a1* and *Slc27a4*, solute carrier family 27 members 1 and 4; *Fabp3*, fatty acid–binding protein 3; *Acsl1*, long-chain fatty acid coenzyme A ligase 1; *Ephx*, epoxide hydrolase; *Alox*, lipoxygenase; *Acadl*, acyl-CoA dehydrogenase; *Hadhb*, hydroxyacyl-CoA dehydrogenase/3-ketoacyl-CoA thiolase/enoyl-CoA hydratase β subunit; *Cpt1b*, carnitine palmitoyltransferase 1b; *Acacb*, acetyl-CoA carboxylase β; 12-HETE, 12*S*-hydroxyeicosatetraenoic acid; 12,13-DiHOME, 12,13-dihydroxyoctadecanoic acid; IPGTT, intraperitoneal glucose tolerance test; IPITT, intraperitoneal insulin tolerance test; ROS, reactive oxygen species; SFA, saturated fatty acid; MUFA, monounsaturated fatty acid; PUFA, polyunsaturated fatty acid; Pparα, proliferator-activated receptor-α; MEM, minimum essential medium; KRH, Krebs-Ringer solution, Hepes-buffered.

Muscle insulin resistance in znt7-KO mice

znt7-KO mice are susceptible to diet-induced insulin resistance. We showed that the abnormality in glucose metabolism was attributed to the disruption of insulin metabolism in pancreatic β-cells in *znt7*-KO mice (4, 6) and reduced insulin sensitivity in skeletal muscle, a tissue responsible for 70–80% of glucose disposal following a carbohydrate load (4). The underlying molecular mechanism by which the *znt7*-null mutation leads to peripheral insulin resistance in *znt7*-knockout mice is still unknown. We reported previously that the *znt7*-null mutation decreased lipid accumulation in mouse adipose tissue (5). Hence, we hypothesized that insulin resistance in the muscle of *znt7*-KO mice might be the result of fat partitioning from adipose to nonadipose tissues. According to the ZnT7 protein expression pattern in the skeletal muscle (abundant) and liver (undetectable in hepatocytes), we further hypothesized that the lipid partitioning in the *znt7*-KO mouse mainly occurred in the skeletal muscle but not the liver.

In this study, we used fatty acid and oxylipin profiling, EM, immunohistochemistry, quantitative RT-PCR, and Western blot analysis to probe the underlying mechanism of insulin resistance in the skeletal muscle of *znt7*-KO mice. Here, we provide evidence that insulin resistance in *znt7*-KO mice is associated with increased uptake and binding of free fatty acids in the muscle cell. Bioactive lipid mediators were elevated in the skeletal muscle of *znt7*-KO mice and showed the potential to drive insulin resistance. In addition, we demonstrated that the fatty acid oxidative capacity of *znt7*-KO muscle cells was increased, evident by the enlarged mitochondria, increased mRNA and protein expression of key enzymes involved in fatty acid mitochondrial shuttle and β-oxidation, and reactive oxygen species (ROS) production.

Results

We previously demonstrated that adult male *znt7*-KO mice were more sensitive to high fat diet–induced abnormalities in glucose and insulin metabolism than the WT control mice (4). We have also shown that *znt7*-KO mice gain less body weight than the controls mainly due to reduced body fat accumulation (10, 11). Hence, we hypothesized that *znt7*-KO mice had dysregulation of lipid metabolism and that this genetically predisposed factor might render the *znt7*-KO mouse sensitive to high fat diet–induced glucose intolerance. We therefore studied a cohort of 18.5-week-old male *znt7*-KO and age-matched male WT littermates to determine the underlying mechanism of insulin resistance in metabolically relevant tissues, such as the skeletal muscle and liver. *znt7*-KO mice used in this study were congenic mice with a C57BL/6J (B6) genetic background in which the *znt7* allele (129P2) was backcrossed to the B6 strain for at least 12 generations. The KO and WT mice were littermates; therefore, both the *znt7*-KO and WT mice were genetically identical except for the *znt7* allele and its flanking regions on chromosome 3.

The study design is laid out in Fig. 1*A*. Both genotypes of mice were fed a semipurified diet containing 30 mg of zinc/kg of diet starting at 5 weeks of age. Difference in body weight was seen around 9–10 weeks of age and became significant at 13 weeks between the two genotype groups (Fig. 1*B*). We observed that mice in both *znt7*-KO and WT groups gained limited weight 1

week after they were singly housed at 11 weeks of age. But the body weight gain resumed from 13 weeks until euthanization at 18.5 weeks (Fig. 1*B*). Table 1 lists the measurements of body weights, fat pad weights, and organ weights at necrosis. As we expected, when compared with the WT controls, *znt7*-KO mice accumulated less body fat as measured by individual or total fat pad weights (epididymal, subcutaneous, and retroperitoneal fat pads). When adjusting the body fat (total measured fat pad weights) to the body weight, *znt7*-KO mice appeared leaner than the WT controls at 18.5 weeks (Table 1), consistent with our previous findings in *znt7*-KO mice with a mixed B6 and 129P2 genetic background (10, 11). The weights of other organs, including the liver, heart, and brain, were not apparently different between the two genotypes (Table 1). Food intake was decreased in the KO group (Fig. 1*C*). However, when the food intake was adjusted for the body weight gain, the food intake per gram of body weight gain was comparable between the two genotype groups (Fig. 1*D*), suggesting a similar growth efficiency.

Overnight fasting plasma triglycerides and cholesterol levels were slightly low in *znt7*-KO mice compared with the WT controls, whereas overnight fasting glucose and total fatty acid levels were similar between the two genotypes (Table 2). In contrast, an elevated blood glucose level (17%, $p < 0.01$) was observed in *znt7*-KO mice compared with the controls after short-term fasting (6 h), suggesting abnormal glucose metabolism in *znt7*-KO mice. Nevertheless, the increased 6-h fasting glucose level in *znt7*-KO mice was not accompanied by an elevated blood insulin level (Table 2). The effect of the *znt7*-KO on the whole-body glucose metabolism was further confirmed by glucose and insulin tolerance tests. As shown in Fig. 2*A*, *znt7*-KO mice had a higher blood glucose level than the controls at 120 min ($p < 0.05$) after a glucose load (Fig. 2*A*). Plasma insulin levels in *znt7*-KO mice during glucose tolerance tests were not significantly changed compared with the controls (Fig. 2*B*). Furthermore, blood glucose levels in *znt7*-KO mice during insulin tolerance tests were higher than those of the controls, suggesting a resistance to the blood glucose-lowering effect of exogenously administered insulin in *znt7*-KO mice (Fig. 2*C*). This resistance was also reflected by the area under the curve glucose measurements of the insulin tolerance test (Fig. 2*D*). Taken together, our data suggest that *znt7*-KO mice had impaired glucose tolerance, likely due to insulin resistance.

The homeostatic control of blood glucose levels is largely accomplished by the skeletal muscle, liver, and adipose tissue in which the muscle takes up and utilizes about 70–80% of daily absorbed glucose (12). We have shown that the activity of the insulin signaling pathway and glucose uptake are compromised by *znt7* knockdown in adipocytes, leading to a reduction in fat accumulation (5). Thus, we hypothesized that fat partitioning from adipose to nonadipose tissues might be the underlying mechanism of insulin resistance observed in *znt7*-KO mice. Hence, we performed metabolomic profiling of fatty acids in the skeletal muscle and liver from *znt7*-KO and the control mice.

As shown in Fig. 3*A*, the total fatty acid content in the skeletal muscle of *znt7*-KO mice was 35% higher than that of the control mice ($p < 0.05$). The *sum* of concentrations of saturated (SFA),
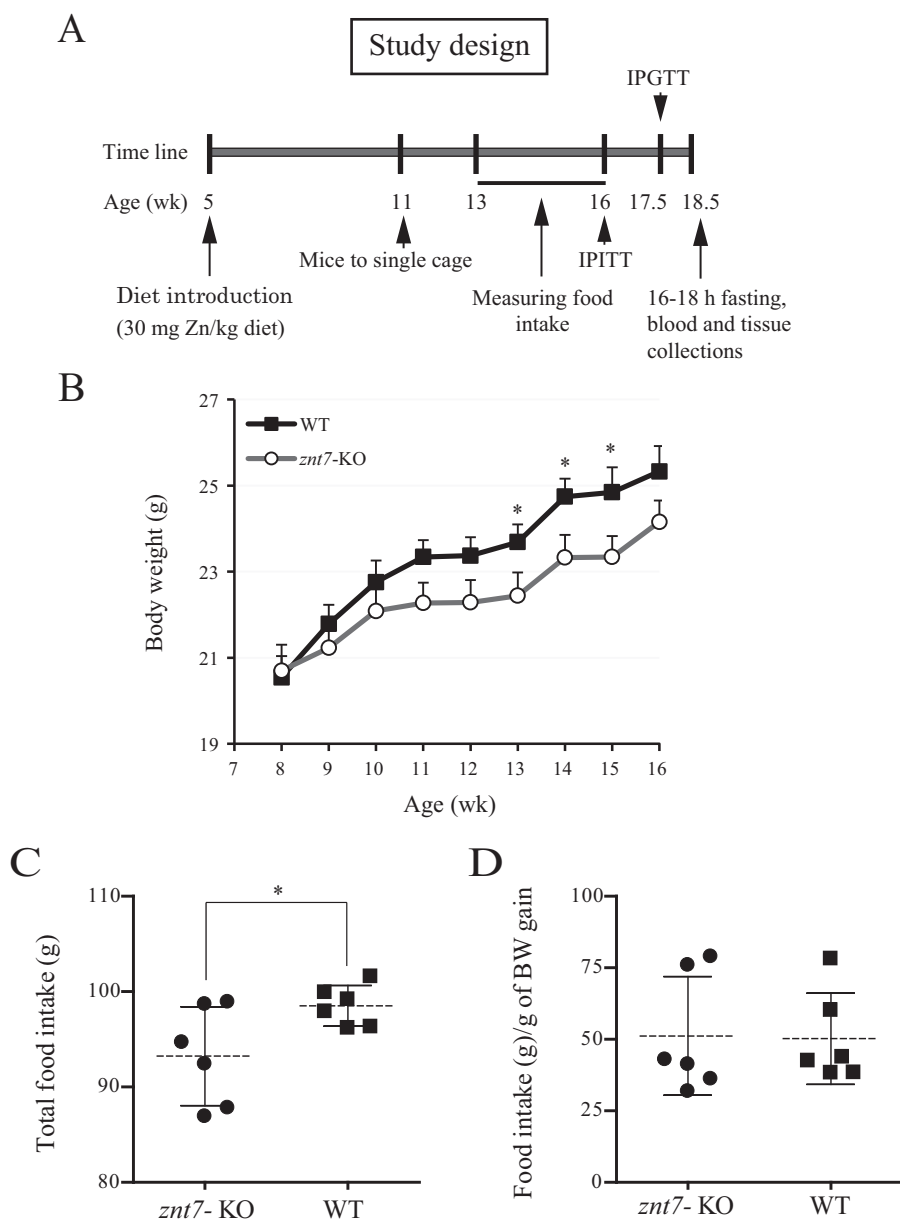
A

Study design

B

C

D

Figure 1. *znt7*-KO mice gained less weight than the WT littermates. *A*, a schematic diagram of the study. Mice were weaned at 3 weeks old. An AIN96-based rodent diet containing 30 mg of zinc/kg of diet was introduced to both *znt7*-KO and control mice at 5 weeks old. All mice were euthanized at 18.5 weeks old. *B*, growth curves during the food intake measuring period. Body weights were monitored for 3 weeks after the special diet was introduced until before the insulin resistance test was performed. *C*, total food (grams) consumed by *znt7*-KO and control mice during the 3-week data collection period. *znt7*-KO and control mice were housed individually at 11 weeks old. Food intake was measured 2 weeks after mice were singly housed. *D*, food intake per gram of body weight gain. *BW*, body weight; *wk*, week; *IPGTT*, intraperitoneal glucose tolerance test; *IPITT*, intraperitoneal insulin tolerance test. Data are means, and *error bars* represent S.D. *, $p < 0.05$.

monounsaturated (MUFA), and polyunsaturated fatty acids (PUFA) was elevated in the skeletal muscle of *znt7*-KO mice compared with that of the controls. The ratio of ω-3 PUFA to ω-6 PUFA was decreased (KO, 0.56 *versus* WT, 0.66), suggesting an increased risk for insulin resistance in the skeletal muscle of *znt7*-KO mice. In addition, fatty acid composition analysis indicated that elevated fatty acids were mostly concentrated in the long-chain fatty acid group (Fig. 3*C*). The relative abundance of C18:1(*n*-9) to C18:0 was increased in the muscle of *znt7*-KO mice ($p = 0.038$), consistent with elevated stearoyl-CoA desaturase 1 activity, which has been reported to contribute to abnormal lipid partitioning and insulin resistance (13).

Arachidonic acid (C20:4(*n*-6)), a key inflammatory intermediate in skeletal muscle (14), was also increased by ∼25% in the *znt7*-KO muscle compared with the controls ($p = 0.029$) (Fig. 3*C*). Meanwhile, the anti-inflammatory docosahexaenoic acid (C22:6(*n*-3)) (15) was increased by ∼30% in the *znt7*-KO muscle compared with the controls ($p = 0.043$). Regardless, the balance of the pro- and anti-inflammatory long-chain fatty acids appeared to be unchanged in the *znt7*-KO muscle ($p = 0.5$). In contrast to the changes observed in the *znt7*-KO muscle, little to no change in the total fatty acid content or composition was observed in the liver of *znt7*-KO compared with the control mice (Fig. 3, *B* and *D*). This discrepancy may be associ-

Muscle insulin resistance in znt7-KO mice

Table 1
Body and tissue weights in *znt7*-KO and WT control mice

	znt7-KO (*n* = 6)	WT (*n* = 6)	*p* value[a]
Body weight (BW)	24.75 ± 0.54	26.10 ± 0.54	0.070
Fat mass (mg)			
Epididymal fat	201.03 ± 13.22	292.25 ± 34.53	0.016*
Femoral subcutaneous fat	161.93 ± 10.95	236.25 ± 19.01	0.003*
Retroperitoneal fat	32.38 ± 5.25	63.22 ± 12.27	0.022*
Percentage of total fat pads to BW	1.80 ± 0.09	2.51 ± 0.24	0.011*
Liver (mg)	871.55 ± 19.74	938.13 ± 44.47	0.101
Percentage of liver to BW	3.98 ± 0.04	3.99 ± 0.19	0.484
Heart (mg)	116.55 ± 5.87	116.00 ± 5.89	0.474
Brain (mg)	378.90 ± 12.30	407.85 ± 10.94	0.055

[a] Student's *t* test was used for calculation of *p* values; *, statistically significant.

Table 2
Blood chemistry parameters in *znt7*-KO and WT control mice

	znt7-KO (*n* = 6)	WT (*n* = 6)	*p* value[a]
Blood glucose, 16 h fasting (mg/dl)	92.67 ± 3.84	87.30 ± 14.69	0.366
Blood glucose, 6 h fasting (mg/dl)	217.17 ± 5.68	185.50 ± 8.84	<0.01*
Plasma insulin, 6 h fasting (ng/ml)	0.35 ± 0.12	0.31 ± 0.03	0.269
Plasma triglycerides, 16 h fasting (mg/dl)	47.06 ± 1.31	51.69 ± 2.17	<0.05*
Plasma cholesterol, 16 h fasting (mg/dl)	71.88 ± 1.67	81.88 ± 3.21	0.05
Plasma total fatty acids, 16 h fasting (mM)	8.50 ± 2.89	7.95 ± 2.99	0.103

[a] Student's *t* test was used for calculation of *p* values; *, statistically significant.

ated with the difference in ZnT7 protein expression levels in the two tissues (Fig. 3, *C* and *D*, *insets*). We showed that ZnT7 was readily detectable in the sarcoplasm of the myofibril, whereas ZnT7 was absent from the hepatocyte. Only the sinusoid endothelial cell in the liver stained positive for ZnT7 (Fig. 3, *C* and *D*, *insets*).

To examine whether increased fatty acid content leads to an increased lipid accumulation in the skeletal muscle of *znt7*-KO mice, we stained the femoral skeletal muscle prepared from *znt7*-KO and WT mice with Oil Red O, a dye that detects neutral lipids. As shown in Fig. 4*A*, lipid accumulation was noticeably increased in the myofibrils of *znt7*-KO mice compared with the controls. This observation was further confirmed by triglyceride quantification in the skeletal muscle of *znt7*-KO and WT mice. We showed that *znt7*-KO skeletal muscle contained ∼50% higher triglycerides than the control (Fig. 4*B*). Together, we conclude that *znt7*-KO impairs lipid metabolism in the skeletal muscle.

Next, we examined whether increased fatty acid concentrations in the skeletal muscle of *znt7*-KO mice would result in an increased capacity for fatty acid utilization. First, we performed EM of the femoral skeletal muscle isolated from *znt7*-KO and WT mice. As shown in Fig. 5*A*, in the WT, the mitochondria (dark and ovoid structures) were localized at the level of the I band and centered around the *z*-line between the myofibrils (16). In contrast, in the *znt7*-KO muscle, the sarcoplasmic space of the myofibril was inflated with nonuniformly distributed mitochondria. In addition, the size of the mitochondria in the *znt7*-KO muscle was expanded, covering two or more *z*-lines along the myofibril (Fig. 5*A*). High magnification images revealed a high level of lipid accumulation between the mito-

chondria in the *znt7*-KO muscle (Fig. 5*B*). Nevertheless, we did not observe a noticeable internal structure change in the mitochondria of the *znt7*-KO muscle (Fig. 5*B*). In addition, mitochondrial DNA contents in the muscle cells between *znt7*-KO and the WT controls were not different (data not shown).

Dysregulation of several factors, such as fatty acid transport, intracellular fatty acid binding, and/or fatty acid oxidation, could increase fatty acid concentrations in the *znt7*-KO muscle. Thus, we decided to investigate the mRNA expression of genes involved in the fatty acid uptake and oxidation in the skeletal muscle, including *Cd36* (fatty acid translocase), *Slc27a1* (long-chain fatty acid transport protein 1), *Slc27a4*, *Fabp3* (fatty acid–binding protein 3), *Acsl1* (long-chain fatty acid CoA ligase 1), *Acacb* (acetyl-CoA carboxylase 2), *Cpt1b* (carnitine palmitoyltransferase 1b), *Acadl* (long-chain acyl-CoA dehydrogenase), and *Hadhb* (3-ketoacyl-CoA thiolase, β subunit), in differentiated primary myoblasts isolated from skeletal muscles of *znt7*-KO and WT mice (4). Although primary isolated skeletal muscle cells might not reflect skeletal muscle *in vivo*, we used these cells to achieve improved results for quantitative PCR, Western blot assay, fatty acid uptake, and ROS measurements. As shown in Fig. 6*A*, among the genes examined, the mRNA expression of *Fabp3*, a gene associated with intracellular fatty acid binding, was significantly higher (25-fold) in the *znt7*-KO primary myotubes than in the WT controls. Up-regulation of Fabp3 in *znt7*-KO myotubes was also confirmed at the protein level (Fig. 6*B*). Four genes that are implicated in fatty acid uptake, *Cd36*, *Slc27a1*, *Slc27a4*, and *Acsl1*, were moderately up-regulated (2.5–5-fold higher in the *znt7*-KO muscle than in the controls). We further confirmed that the up-regulation of expression of these fatty acid uptake genes in *znt7*-KO myotubes led to an increase in fatty acid uptake by ∼27% compared with the controls (Fig. 6*C*). Interestingly, the mRNA expression of *Acacb*, an enzyme that converts acetyl-CoA to malonyl-CoA, was also up-regulated in the *znt7*-KO primary myotubes. Malonyl-CoA is a potent inhibitor of mitochondrial fatty acid uptake through allosteric inhibition of Cpt1 enzymatic activity, a rate-limiting step in fatty acid uptake and oxidation by the mitochondria. Increased mRNA expression of *Acacb* suggests a negative impact of the *znt7*-KO on mitochondrial fatty acid oxidation in myotubes even though *Acadl* and *Hadhb* were up-regulated in the *znt7*-KO primary myotubes compared with the controls (Fig. 7, *A* and *B*). Taken together, our results suggest that the *znt7*-null mutation may increase fatty acid uptake and expand the Fabp3-bound fatty acid pool in the skeletal muscle. *znt7*-KO may also impair fatty acid oxidation in the skeletal muscle. As a result, lipids accumulate in the skeletal muscle of *znt7*-KO mice.

To determine whether high intracellular fatty acid levels in *znt7*-KO muscle cells would result in oxidative stress, we examined mRNA expression of genes associated with oxidative stress and inflammation, such as *Alox5* (arachidonate 5-lipoxygenase), *Alox12* (arachidonate 12-lipoxygenase), *Alox15* (arachidonate 15-lipoxygenase), and *Ephx1–4* (epoxide hydrolases 1–4) in primary *znt7*-KO and WT myotubes. We also examined oxylipin contents in skeletal muscles isolated from *znt7*-KO and WT mice. As shown in Fig. 7*C*, quantitative RT-PCR analyses showed that *znt7*-KO myotubes had a 25-fold
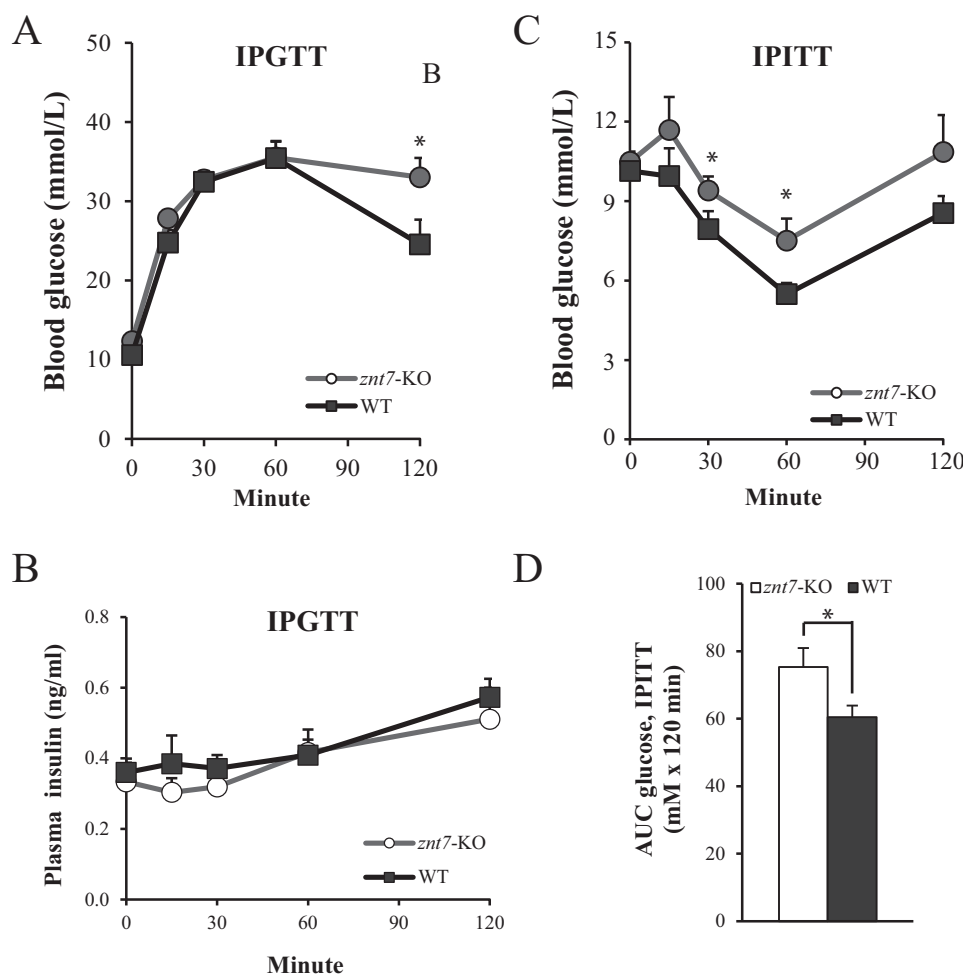
Figure 2. Intraperitoneal glucose and insulin tolerance tests. *A*, blood glucose levels during IPGTT. *B*, plasma insulin levels during IPGTT. *C*, blood glucose levels during IPITT. *D*, the area under the curve (*AUC*) for glucose concentrations during IPITT. Both *znt7*-KO and WT mice were fasted 6 (IPGTT) or 4 h (IPITT) at 7:00 a.m. before the test. Blood was collected at the indicated time points before and after administration of glucose or insulin. Values are means, and *error bars* represent S.E., $n = 6$ per genotype of mice. *, $p < 0.05$.

increase in *Alox12* mRNA expression, whereas no significant difference in the expression of *Alox5* and *Alox15* was seen (data not shown). Moreover, in *znt7*-KO primary myotubes, the mRNA expression of all *Ephx* genes except *Ephx3* was up-regulated. The oxidative status of *znt7*-KO in muscle cells was further illustrated by ROS levels in living cells. As shown in Fig. 7D, a higher ROS level (2.2-fold, $p < 0.01$) was detected in *znt7*-KO myotubes than in the WT control cells.

Oxylipins are bioactive lipids, and elevations in these compounds are often associated with oxidative stress and inflammation (17). We showed that *znt7*-KO skeletal muscle had increased levels of linoleic acid, α-linolenic acid, and arachidonic acid (Fig. 3C). The mRNA expression of genes that encode enzymes involved in metabolizing these fatty acids to oxylipins, including lipoxygenases and epoxide hydrolases, were also up-regulated (Fig. 7C). We next investigated the nonesterified oxylipin pool of femoral skeletal muscle isolated from *znt7*-KO and WT mice. We found that 14 oxylipins among metabolites examined, including both *n*-6– and *n*-3–derived compounds, were significantly higher in the *znt7*-KO skeletal muscle than those of the control (Fig. 8A). Although their relative potencies can be argued, 10 of these

oxylipins have been associated with oxidative stress or inflammation (Table 3). In addition, four metabolites were found to be slightly lower in concentration in the muscle of *znt7*-KO mice than that in the control (Fig. 8A).

To better understand the relationship between increased oxylipins and insulin resistance, we investigated metabolites from two distinct biosynthesis cascades with plausible links to glucose regulation, specifically, modulation of insulin signaling and glucose uptake by 12,13-dihydroxyoctadecanoic acid (12,13-DiHOME; a product of the soluble epoxide hydrolase) and 12-hydroxyeicosatetraenoic acid (12-HETE; a product of 12-lipoxygenase) in rat L6 myotubes. A decrease in the activity of the insulin signaling pathway is a signature of insulin resistance in skeletal muscle cells. Thus, we examined phosphorylation levels of Akts, a key step in modulation of insulin signaling and translocation of Glut4 from an intracellular storage pool to the cytoplasmic membrane for glucose uptake. L6 myotubes were treated with either 12,13-DiHOME (2 μM) or 12-HETE (2 μM) for 18 h. As shown in Fig. 8, *B and C*, the insulin-dependent phosphorylation of Akts was decreased by 40 and 35% in L6 myotubes treated with 12,13-DiHOME and 12-HETE, respectively, compared
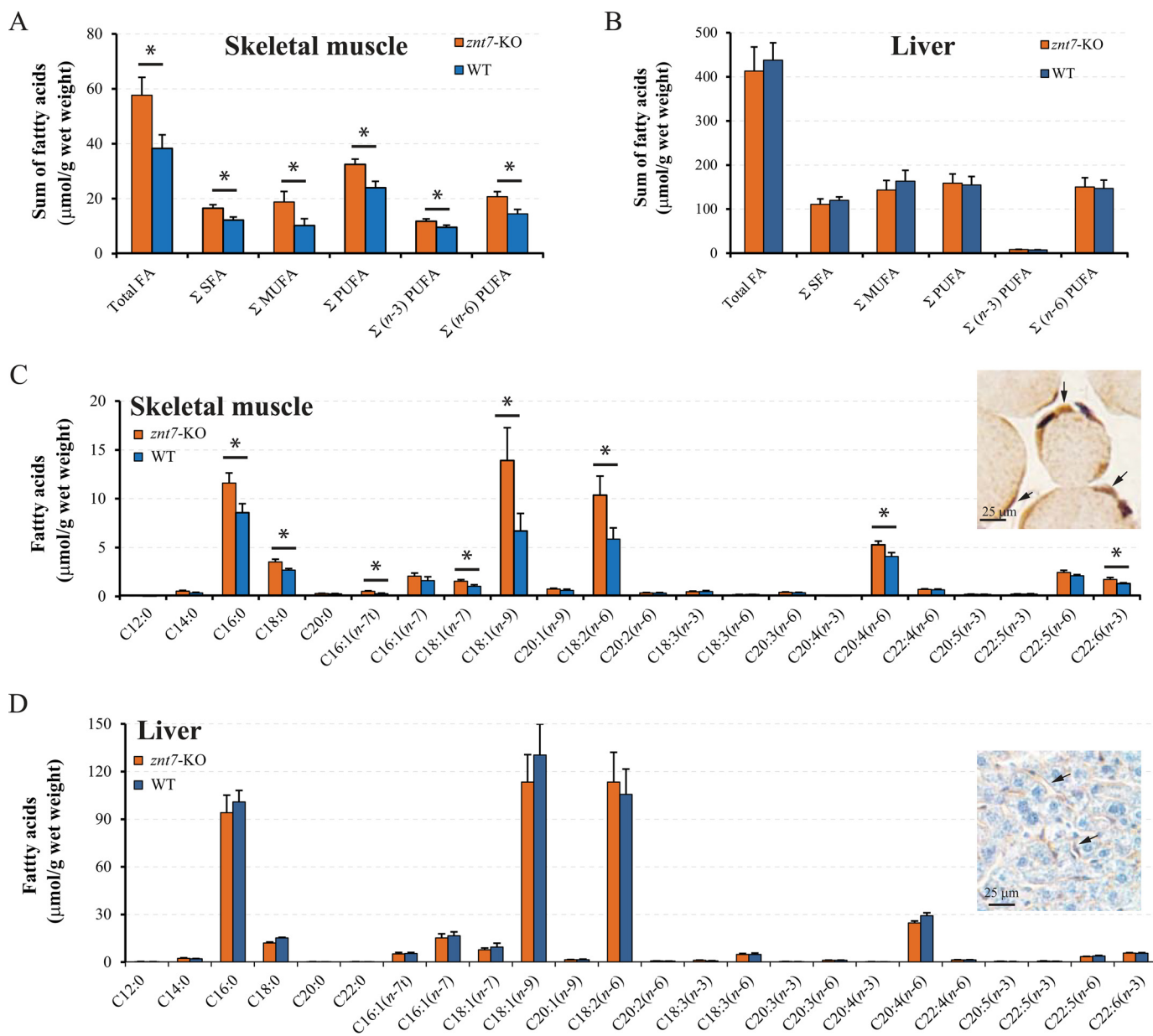
Figure 3. Fatty acid profiling in the skeletal muscle and liver of *znt7*-KO and WT mice. Skeletal muscle and liver were collected from *znt7*-KO and control mice at 18.5 weeks old after overnight fasting (16–18 h). Total fatty acids, total saturated fatty acids (ΣSFA), total monounsaturated fatty acids (ΣMUFA), total polyunsaturated fatty acids (ΣPUFA), total ω-3 polyunsaturated fatty acids (Σ(n-3)PUFA), and total ω-6 polyunsaturated fatty acids (Σ(n-6)PUFA) were calculated by the sum of the fatty acids quantified (see "Experimental procedures" for details). *A*, fatty acid contents in the skeletal muscle. *B*, fatty acid contents in the liver. *C*, fatty acid compositions in the skeletal muscle. The *inset* is a representative photograph of immunohistochemical staining of ZnT7 in the mouse skeletal muscle. *Arrows* indicate ZnT7 in the myofibrils. *D*, fatty acid compositions in the liver. The *inset* is a representative photograph of immunohistochemical staining of ZnT7 in the mouse liver. ZnT7 is expressed in the hepatic sinusoid (*arrows*) but not in the hepatocyte. Values are means, and *error bars* represent S.E., $n = 6$ per genotype of mice. *, $p < 0.05$.

with vehicle-treated cells. Accordingly, insulin-stimulated glucose uptake was down in the L6 myotubes treated with 12,13-DiHOME and 12-HETE (Fig. 8D). Interestingly, 12,13-DiHOME treatment also lowered the basal glucose uptake in L6 myotubes (Fig. 8D). It is known that the proinflammatory cytokine Ccl2 (also called Mcp1) is a prominent inducer of insulin resistance in skeletal muscle through inhibition of insulin-stimulated Akt phosphorylation and subsequent glucose uptake at a dose above 200 pg/ml in cells (18). We next examined whether L6 myotubes treated with either 12,13-DiHOME or 12-HETE would increase Ccl2 secretion into the culture medium. As shown in Fig. 8E, treatment of

L6 myotubes with either 12,13-DiHOME or 12-HETE was able to induce Ccl2 secretion to a level much higher than 200 pg/ml, suggesting the presence of a negative impact of 12,13-DiHOME or 12-HETE on glucose uptake in muscle cells via Ccl2. Taken together, we conclude that ZnT7 and thus intracellular zinc play an important role in lipid metabolism of the skeletal muscle. The *znt7* knockdown increased intracellular fatty acid levels in the skeletal muscle; led to up-regulation of *Alox12*, *Ephx1*, *Ephx2*, and *Ephx4* gene expression; and promoted downstream fatty acid metabolite production, modulating insulin signaling in the skeletal muscle of *znt7*-KO mice (Fig. 9).
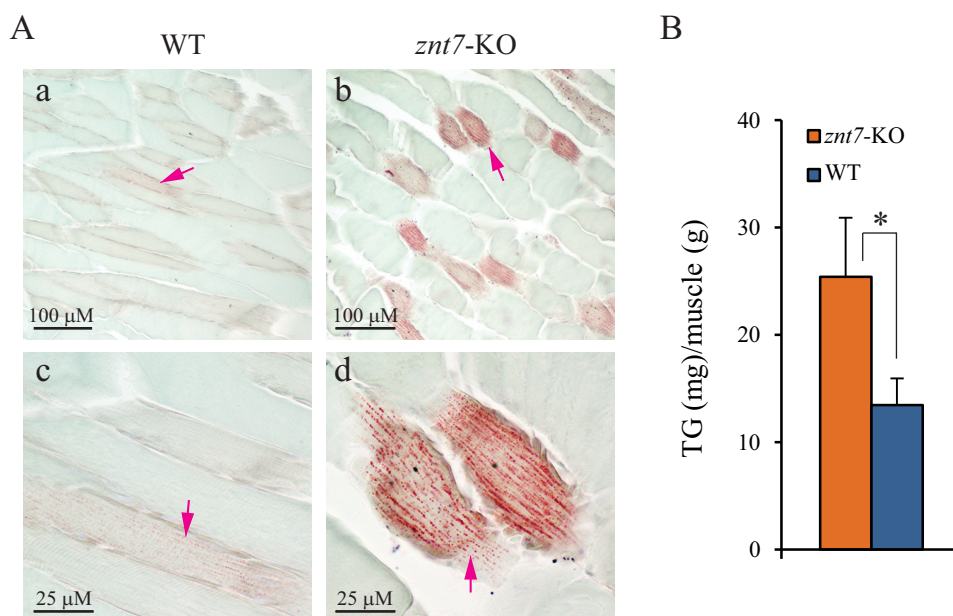
Figure 4. Lipid accumulation in the skeletal muscle of *znt7*-KO mice. Skeletal muscle was isolated from *znt7*-KO and control mice at 18.5 weeks old after 16–18-h fasting. *A, panels a–d,* intracellular lipid accumulation in the myofibril of *znt7*-KO and control mice. Neutral lipids and triglycerides in the skeletal muscle were stained by Oil Red O. *Arrows* indicate the location of lipids stained by Oil Red O. *B,* quantification of triglycerides (*TG*) in the skeletal muscle. Triglycerides in the muscle protein lysate were determined using an L-Type Triglyceride M kit. Values are means, and *error bars* represent S.E., $n = 6$ per genotype of mice. *, $p < 0.05$.

Discussion

It is known that reduced storage of fat in adipose tissue results in greater partitioning of dietary lipids to nonadipose tissues, such as skeletal muscle and liver, causing fat deposition in these tissues (19). We previously demonstrated that *znt7*-KO disrupted lipid accumulation in adipose tissue (5). Thus, we hypothesized that lipid partitioning from adipose tissue to nonadipose tissues triggered insulin resistance in peripheral tissues of *znt7*-KO mice (4). We investigated fatty acid profiles in the skeletal muscle, liver, and plasma isolated from male 18.5-week-old *znt7*-KO and WT littermates. We found significant abnormality in fatty acid metabolism in the skeletal muscle of *znt7*-KO mice, whereas little alteration was found in the liver (Fig. 3*D*) and plasma (data not shown) of *znt7*-KO mice. These abnormalities were characterized by a general increase in tissue lipids with a 2-fold increase in the stearoyl-CoA desaturase activity index (20). This suggests an adaptive shift in metabolism toward lipid storage (21). We showed that the abnormality in fatty acid metabolism in the skeletal muscle of *znt7*-KO mice was in accordance with the expression of ZnT7 protein, which was abundantly expressed in the skeletal muscle with little to no expression in hepatocytes of the liver (Fig. 3, *C* and *D*). Thus, our data support not only that ZnT7 promotes fat storage in adipose tissue but that it is also involved in regulating fatty acid metabolism in the skeletal muscle.

In the heart and skeletal muscle, long-chain fatty acids are taken up by Cd36 and/or Slc27a1/Slc27a4 and subsequently bound to Fabp3 (22). The binding of fatty acids to Fabp3 provides a positive feedback loop in which more long-chain fatty acids are transported into the muscle fibrils (23). Fabp3 functions as an intracellular chaperone to transport fatty acids to appropriate intracellular compartments for β-oxidation, lipid synthesis, and lipid bioactive mediator production (Fig. 9). It

has been demonstrated that Fabp3 is required for oxidation of exogenous fatty acids in the muscle, and the Fabp3 expression level in adipocytes was strongly correlated with obesity development (24). In the skeletal muscle, *Fabp3* mRNA expression is induced in response to an increased dietary fat load in mice leading to lipid accumulation in the skeletal muscle (24–26). Because Fabp3 mRNA and protein expression is markedly increased in the *znt7*-KO skeletal muscle, accompanied by increased expression of fatty acid transporters and long-chain fatty acid CoA ligase 1, we postulate that elevated concentrations of intracellular fatty acid; intracellular lipid deposit; and linoleic acid–, α-linolenic acid–, and arachidonic acid–derived bioactive lipid mediators are elicited by the Fabp3-dependent influx of long-chain fatty acids in the *znt7*-KO muscle fibril. Increased intracellular fatty acid concentrations also up-regulated catabolic/fasting-type metabolism in the *znt7*-KO muscle cells, evident by the extended and enlarged mitochondria and increased gene/protein expression of key enzymes involved in the long-chain fatty acid shuttle between the sarcoplasm and mitochondria and in mitochondrial β-oxidation. This reprogramming in the *znt7*-KO skeletal muscle is suspected to increase the rate of β-oxidation to reduce lipotoxicity, but we have not directly measured this effect.

In addition to the robust up-regulation of *Fabp3* mRNA expression in the *znt7*-KO muscle cell (25-fold higher than the control), we detected a similar rigorous expression pattern for *Alox12* transcripts in the *znt7*-KO muscle cell (25-fold increase compared with the controls). Alox12 is a nonheme iron-containing dioxygenase involved in converting polyunsaturated fatty acids to specific hydroperoxide analogs (*e.g.* arachidonic acid to 12S-hydroperoxyeicosatetraenoic acid), which leads to the downstream production of a spectrum of bioactive lipid mediators involved in inflammatory regulation (27). Although
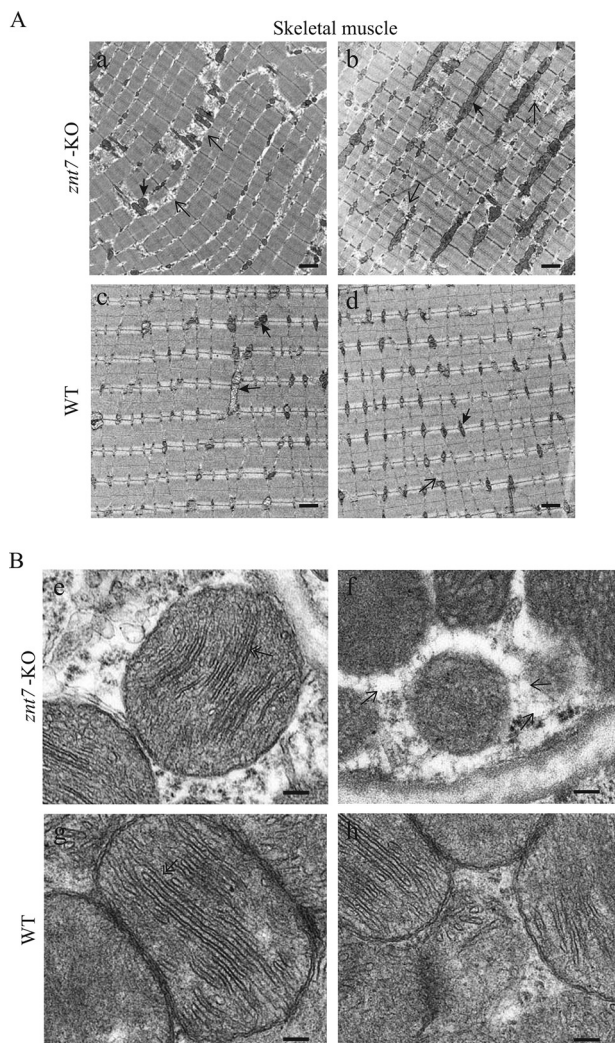
A

B

Figure 5. Electron micrographs of the skeletal muscle from *znt7*-KO and WT mice. *A*, low magnification of electron micrographs. *Panels a and b*, the electron microscopic views of the *znt7*-KO skeletal muscle. Nonuniform distribution of mitochondria was observed. Enlarged mitochondria and expanded sarcoplasm were also noticeable. *Panels c and d*, the electron microscopic views of the WT skeletal muscle. The *solid* and *open arrows* indicate the mitochondria and the sarcoplasm, respectively. *Scale bars*, 1 μm. *B*, high magnification of electron micrographs. *Panels e and f*, the electron microscopic views of the *znt7*-KO skeletal muscle. Abundant lipid droplets were observed. The *open arrows* in *panel f* indicate lipid droplets in the sarcoplasm. *Panels g and h*, the electron microscopic views of the WT skeletal muscle. The *double-headed arrows* in *panels e and g* indicate the double leaflet structure of the mitochondria. *Scale bars*, 0.1 μm.

A

B

C

^{14}C-PA uptake (nmole/mg protein/min)

Figure 6. Expression of *Cd36*, *Slc27a1*, *Slc27a4*, *Acsl1*, and *Fabp3* and [1-^{14}C]palmitic acid uptake in primary skeletal myotubes. *A*, expression of *Cd36*, *Slc27a1*, *Slc27a4*, *Acsl1*, and *Fabp3* mRNAs. Primary myoblasts of *znt7*-KO and the WT control were allowed to differentiate for 4–6 days before harvest. The amount of the target mRNA was measured by SYBR-based quantitative RT-PCR. *Actb* was used as the internal reference, and three independent experiments, each with duplicate or triplicate, were performed. *B*, effect of *znt7*-KO on the protein expression level of Fabp3 in primary myotubes. Primary myoblasts of *znt7*-KO and the WT control were allowed to differentiate for 4 days before harvest. Three micrograms of total proteins were loaded for the Western blot assay. Actb was used as the loading control. Similar results were obtained from multiple experiments, and a representative image is shown. *C*, [^{14}C]palmitic acid (*PA*) uptake. Differentiated primary myotubes were incubated with 80 μM [1-^{14}C]palmitic acid for 0 or 3 min at 37 °C in 5% CO$_2$. The panel shows the palmitate uptake as nmol/mg of protein/min. Results are presented as means, and *error bars* represent S.D. from three independent experiments, each with three to six replicates. *, $p < 0.05$; **, $p < 0.01$.

further studies are warranted, our findings suggest that insulin resistance in the skeletal muscle of *znt7*-KO mice is due to the up-regulation of Fabp3 and subsequently increased levels of bioactive lipid mediators involved in oxidative stress and inflammation. Our results also provide an intriguing clue with respect to a potential molecular marker for intracellular dysregulation of zinc homeostasis.

It appears that increased fatty acid concentrations in the *znt7*-KO skeletal muscle cell provoke a compensatory mechanism to effectively metabolize fatty acids and to avoid lipotoxicity in the muscle. We observed that the mitochondria were enlarged and expanded in the *znt7*-KO skeletal muscle cells, and mRNA or protein expression of key enzymes involved in mitochondrial transport of fatty acids and subsequent β-oxida-
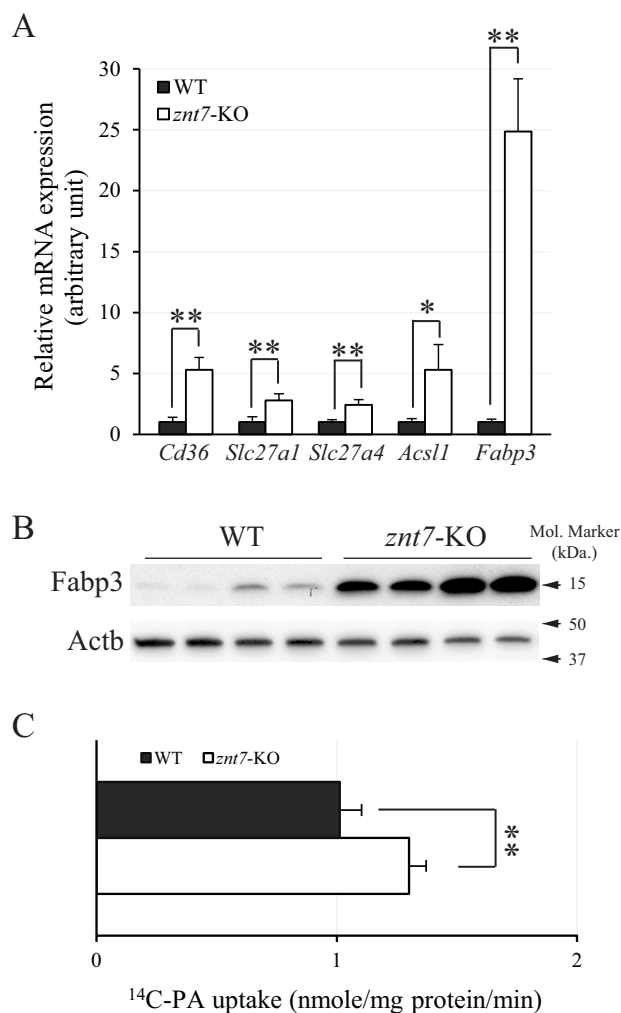
tion, including *Acadl*, *Cpt1b*, and *Hadhb*, were up-regulated. However, the increased capacity was outpaced by fatty acid uptake. Thus, the excessive fatty acids were deposited as triglycerides in the *znt7*-KO skeletal muscle, leading to high intracellular lipid accumulation. From our oxylipin profiling result, it is evident that *znt7*-KO muscle cells had elevated levels of mediators associated with either inflammation or oxidative stress (Table 3). Our results in mRNA expression of *Ephx1*, *Ephx2*, and *Ephx4*; ROS production in *znt7*-KO primary myotubes; and Ccl2 secretion from oxylipin-treated L6 myotubes support the notion that *znt7*-KO skeletal muscle was under
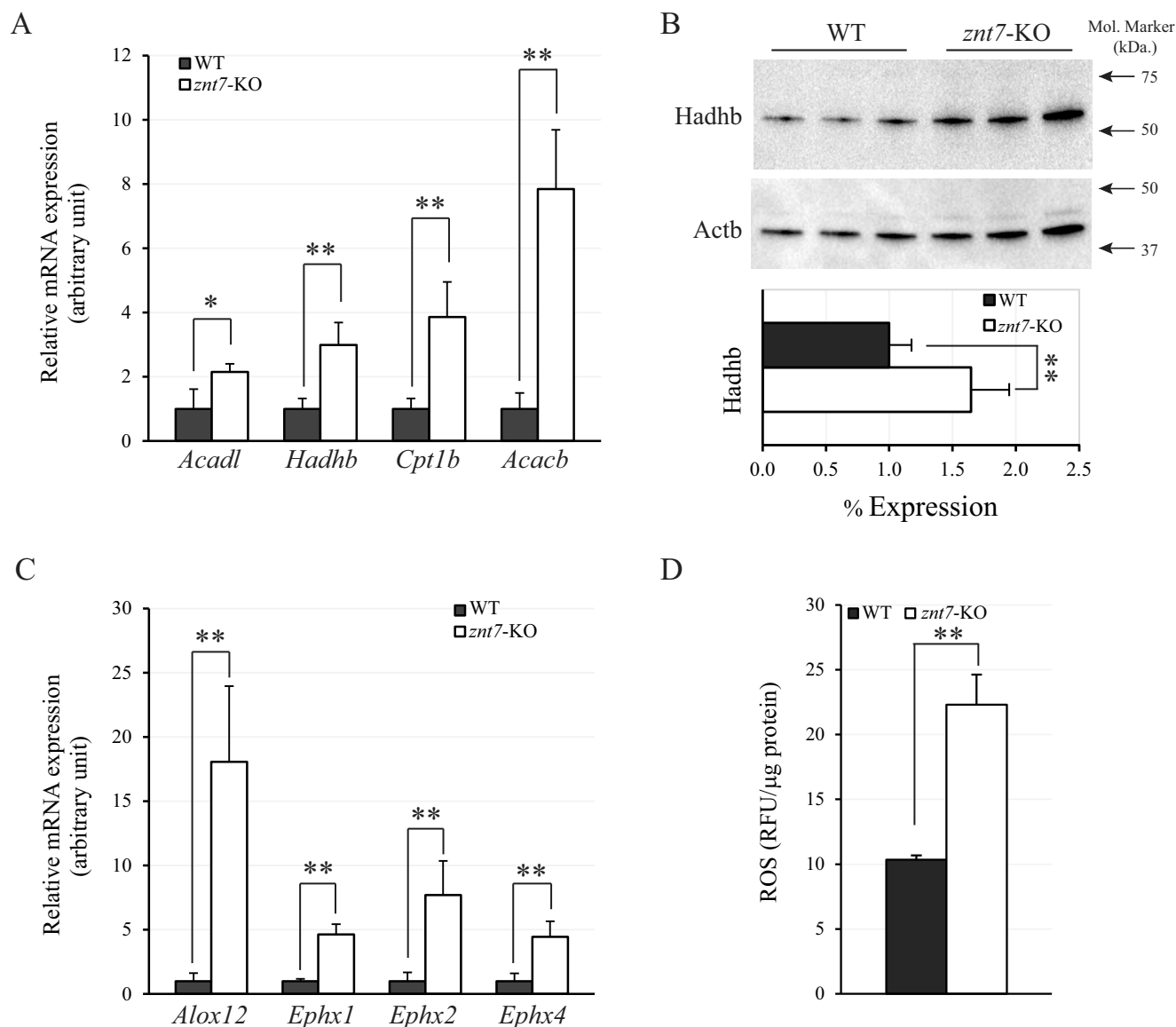
A

B

C

D

Figure 7. Expression of key enzymes involved in the mitochondrial β-oxidation, bioactive lipid mediator production, and ROS accumulation in primary skeletal myotubes. *A*, expression of *Acadl*, *Hadhb*, *Cpt1b*, and *Acacb* mRNAs. *B*, expression of Hadhb protein. *C*, expression of *Alox12*, *Ephx1*, *Ephx2*, and *Ephx4* mRNAs. Primary myoblasts of *znt7*-KO and the WT control were allowed to differentiate for 4–6 days before the experiments. The amount of the target mRNA was measured by SYBR-based quantitative RT-PCR. Three micrograms of total proteins were loaded for the Western blotting assay. *Actb* was used as the internal reference for mRNA measurements or as the loading control for Western blotting assays. Three independent experiments, each with duplicate or triplicate, were performed. A representative image of the Western blot assays is shown. *D*, ROS levels in living myotubes. Results are means, and *error bars* represent S.E. (three independent experiments with three to six replicates, $n = 12$). *RFU*, relative fluorescence units, excitation/emission, 540/570 nm. *, $p < 0.05$; **, $p < 0.01$.

oxidative stress, which activates inflammatory pathways, leading to insulin resistance in *znt7*-KO mice.

It is noteworthy that, in the *znt7*-KO skeletal muscle, up-regulation of *Fabp3* mRNA expression was highly and positively correlated with the change in *Alox12* mRNA expression but not *Alox5* or *Alox15* mRNA expression (data not shown). One may speculate that the promoters of *Fabp3* and *Alox12* genes share one or more regulatory elements for transcription factors that are sensitive to change in intracellular zinc concentrations in the skeletal muscle. By searching the database for transcriptional factor–binding sites in promoters provided by MAPPER2 (multigenome analysis of positions and patterns of elements of regulation), we found that the promoter regions of *Fabp3* and *Alox12* (2000 bp upstream of the transcriptional start sites)

share many potential transcriptional factor–binding sites (28). Among them, paired box protein (Pax6)– and peroxisome proliferator-activated receptor-α (Pparα)–binding sequences are commonly present in the promoters of *Fabp3* and *Alox12* but not in those of *Alox5* and *Alox15*. Pax6 is a transcriptional factor that plays key roles in the development of neural tissues. The null mutation in the *Pax6* gene causes severe defects in eye development in mice. Pax6 also regulates glucagon gene expression in the pancreatic islet implicated in glucose metabolism. Thus, it is not surprising that *Fabp3* and *Alox12* are target genes for Pax6. Pparα is a nuclear hormone receptor transcription factor that is involved in regulating fatty acid oxidation in the heart and skeletal muscle (29). Pparα expression is positively correlated with gene expression of crucial enzymes

involved in fatty acid transport, fatty acid mitochondrial shuttle, and mitochondrial energy production (30). Further exploration of the effect of Pax6 and Pparα on the transcription of *Fabp3* and *Alox12* is required.

In conclusion, the *znt7*-null mutation resulted in altered fatty acid metabolism in skeletal muscle. Increased fatty acid accu-

mulation in the *znt7*-KO muscle cell triggered compensatory mechanisms to oxidize excessive fatty acids in the mitochondria, leading to an expansion of the mitochondria and induction of key enzymes required for mitochondrial β-oxidation. Excessive intracellular fatty acids in the *znt7*-KO muscle cell also increased production of ROS and PUFA-derived mediators of
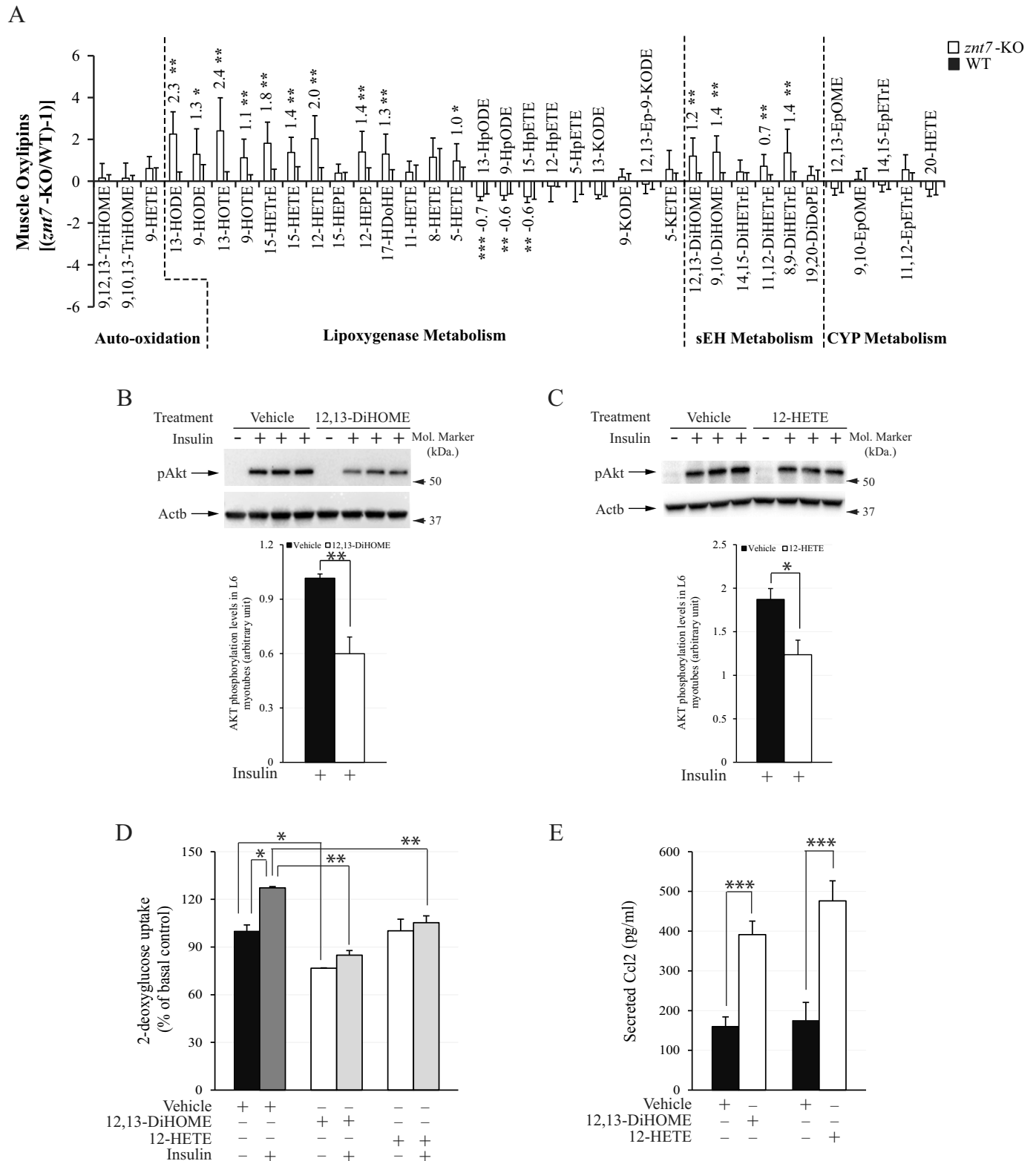
Table 3

Up-regulated oxylipins in the skeletal muscle of *znt7*-KO mice

5-HETE, 5-hydroxyeicosatetraenoic acid; 9-HODE, 9-hydroxyoctadecadienoic acid; 9-HOTE, 9-hydroxyocatadecatrienoic acid; 13-HODE, 13-hydroxyoctadecdienoic acid; 13-HOTE, 13-hydroxyoctadecatrienoic acid; 15-HETE, 15-hydroxyeicosatetraenoic acid; 12-HEPE, 12-hydroxyeicosapentaenoic acid; 17-HDoHE, 17-hydroxydoco-sahexaenoic acid; 9,10-DiHOME, 9,10-dihydroxyoctadecanoic acid; 11,12-DiHETrE, 11,12-dihydroxyeicosatrienoic acid; 8,9-DiHETrE, 5,11,14-eicosatrienoic acid.

Metabolite	Precursor fatty acid	Enzyme involved	Relevant biological significance to this study[a]
5-HETE	Arachidonic acid	Lipoxygenase	Inflammation
9-HODE	Linoleic acid	Lipoxygenase	Oxidative stress
9-HOTE	α-Linolenic acid	Lipoxygenase	Unknown
13-HODE	Linoleic acid	Lipoxygenase	Oxidative stress
13-HOTE	α-linolenic acid	Lipoxygenase	Unknown
15-HETrE	Dihomo-γ-linolenic acid	Lipoxygenase	Oxidative stress
15-HETE	Arachidonic acid	Lipoxygenase	Inflammation
12-HETE	Arachidonic acid	Lipoxygenase	Inflammation
12-HEPE	Eicosapentaenoic acid	Lipoxygenase	Unknown
17-HDoHE	Docosahexaenoic acid	Lipoxygenase	Oxidative stress
12,13-DiHOME	Linoleic acid	P450/epoxide hydrolase	Oxidative stress
9,10-DiHOME	Linoleic acid	P450/epoxide hydrolase	Oxidative stress
11,12-DiHETrE	Arachidonic acid	P450/epoxide hydrolase	Unknown
8,9-DiHETrE	Arachidonic acid	P450/epoxide hydrolase	Inflammation

[a] Information was obtained from the KEGG database or the Metabolomics Innovation Center.

oxidative stress and inflammation, leading to muscle insulin resistance in *znt7*-KO mice.

Experimental procedures

Animals and diets

The generation and characterization of *znt7*-KO mice were described previously (4, 10). Both *znt7*-KO and WT littermates were generated from heterozygous mating. Male mice with desired genotypes were weaned at 3 weeks old and fed a semi-purified diet containing 30 mg of zinc/kg of diet (Research Diets, New Brunswick, NJ) *ad libitum* from 5 to 18.5 weeks. At 11 weeks old, mice were singly housed, and food consumption was measured every other day from 13 to16 weeks. At the end of the study, mice were fasted (16–18 h) and euthanized. Blood and tissues, including skeletal muscle and liver, were collected for subsequent experiments. All mice were housed in a temperature-controlled room at 22–24 °C with a 12-h light:dark cycle. Breeding mice were fed a standard laboratory chow diet (Laboratory Rodent Diet 5001, LabDiet, Brentwood, MO) and dou-ble-distilled water *ad libitum*. All animal experiments were conducted in accordance with National Institutes of Health Guidelines for the Care and Use of Experimental Animals and were approved by the Institutional Animal Care and Use Committee of the University of California, Davis.

Genotyping

Genotyping was performed as described previously using tail clips (10).

Intraperitoneal glucose tolerance test

Before the test, mice were fasted for 6 h. Mice were weighed, and glucose (1.5 g/kg of body weight) was given intraperitoneally. Blood was collected from the tail vein at 0, 15, 30, 60, and 120 min after glucose administration. Blood glucose and plasma insulin levels were determined using a One-Touch UltraMini meter (LifeScan) and a mouse ultrasensitive insulin ELISA kit (Alpco), respectively.

Figure 8. Oxylipin profiling of skeletal muscle of *znt7*-KO and the controls and effects of oxylipins on insulin signaling and cytokine secretion in L6 muscle cells. *A*, oxylipin profiling of the *znt7*-KO and WT skeletal muscle. Femoral skeletal muscle tissues were isolated from *znt7*-KO and control mice at 18.5 weeks old after 16–18 h fasting. Oxylipin concentrations were measured as described under "Experimental procedures." Among the metabolites examined, 14 oxylipins were significantly higher in the *znt7*-KO skeletal muscle than the WT controls. Values are means, and *error bars* represent S.E., $n = 6$ per genotype. Metabolites were grouped in their metabolic pathways. *sEH*, epoxide hydrolase; *CYP*, cytochrome p450; *9,12,13-TriHOME*, 9,12,13-trihydroxyoctadecenoic acid; *9,10,13-TriHOME*, 9,10,13-trihydroxyoctadecenoic acid; *9-HETE*, 9-hydroxyeicosatetraenoic acid; *13-HODE*, 13-hydroxyoctadecadienoic acid; *9-HODE*, 9-hydroxyoctadecadienoic acid; *13-HOTE*, 13-hydroxyoctadecatrienoic acid; *9-HOTE*, 9-hydroxyocatadecatrienoic acid; *15-HETrE*, 15-hydroxyeicosatrienoic acid; *15-HETE*, 15-hydroxyeicosatetraenoic acid; *15-HEPE*, 15-eicosapentaenoic acid; *12-HEPE*, 12-hydroxyeicosapentaenoic acid; *17-HDoHE*, 17-hydroxydoco-sahexaenoic acid; *11-HETE*, 11-hydroxyeicosatetraenoic acid; *8-HETE*, 8-hydroxyeicosatetraenoic acid; *5-HETE*, 5-hydroxyeicosatetraenoic acid; *13-HpODE*, 13-hy-droxyoctadecadienoic acid; *9-HpODE*, 9-hydroxyoctadecadienoic acid; *15-HpETE*, 15-hydroperoxyeicosatetraenoic acid; *12-HpETE*, 12-hydroperoxyeicosatet-raenoic acid; *5-HpETE*, 5-hydroperoxyeicosatetraenoic acid; *13-KODE*, 13-oxooctadecadienoic acid; *9-KODE*, 9-oxooctadecadienoic acid; *12,13-Ep-9-KODE*, 12,13-epoxyoxo-9-octadecenoic acid; *5-KETE*, 5-oxoeicosatetraenoic acid; *9,10-DiHOME*, 9,10-dihydroxyoctadecanoic acid; *14,15-DiHETrE*, 14,15-dihydroxyei-cosatrienoic acid; *11,12-DiHETrE*, 11,12-dihydroxyeicosatrienoic acid; *8,9-DiHETrE*, 8,9-dihydroxyeicosatrienoic acid; *19,20-DiHDoPE*, 19,20-dihydroxydocosap-entaenoic acid; *12,13-EpOME*, 12,13-epoxyoctadecenoic acid; *9,10-EpOME*, 9,10-epoxyoctadecenoic acid; *14,15-EpETrE*, 14,15-epoxyeicosatrienoic acid; *11,12-EpETrE*, 11,12-epoxyeicosatrienoic acid; *20-HETE*, 20-hydroxyeicosatetraenoic acid. *B* and *C*, phosphorylation of Akts. L6 myotubes (6×10^4) were treated with 2 μM 12,13-DiHOME (*B*) or 2 μM 12-HETE (*C*) at 37 °C for 18 h and then serum-starved for 2 h followed by insulin stimulation (100 nM) at 37 °C for 7 min. Representative Western blots are displayed. Densitometry of the phosphorylated Akt (*pAkt*) band in the blots was determined and is shown under the Western blot images. Treatment of L6 myotubes with 12,13-DiHOME and 12-HETE caused 40 and 35% reduction, respectively, in insulin-stimulated Akt phosphoryla-tion. *D*, 2-[³H]deoxyglucose uptake in L6 myotubes. Myotubes were treated with 2 μM 12,13-DiHOME or 2 μM 12-HETE at 37 °C for 18 h followed by 2-[³H]de-oxyglucose uptake in the presence of 0 or 100 nM insulin at 37 °C for 15 min. Cells were then washed and lysed for radioactive determinations. Treatment of L6 myotubes with 12,13-DiHOME inhibited glucose uptake by 23% in the basal condition compared with the mock-treated cells. No significant reduction was observed in glucose uptake in L6 myotubes treated with 12-HETE. Insulin treatment of L6 myotubes increased glucose uptake by 27% in the control L6 myotubes. However, this insulin-stimulated glucose uptake was not observed in the L6 myotubes treated with either 12,13-DiHOME or 12-HETE. *E*, secreted Ccl2 from L6 myotubes. L6 myoblasts (6×10^4) were differentiated for 7 days and then treated with 10 μM 12,13-DiHOME or 10 μM 12-HETE at 37 °C for 2 days. Secreted Ccl2 in the supernatant was then determined. L6 myotubes treated with 12,13-DiHOME and 12-HETE increased Ccl2 secretion by 2.4- and 2.7-fold, respectively, compared with the mock-treated controls. All data are reported in *B–E* as means, and *error bars* represent S.D., $n = 3$ per treatment. *, $p < 0.05$; **, $p < 0.01$; ***, $p < 0.001$.
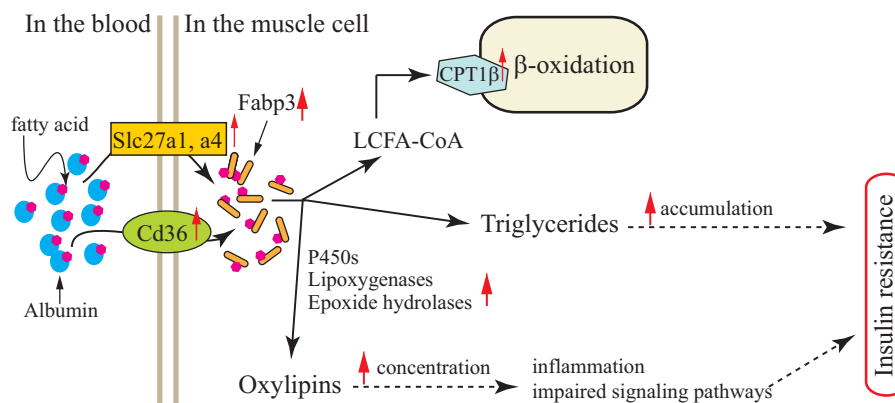
Figure 9. A schematic diagram of fatty acid metabolism and pathways leading to insulin resistance in the *znt7*-KO muscle cell. In the skeletal muscle cell, long-chain fatty acids are taken up by Cd36, Slc27a1, and Slc27a4. Once fatty acids are brought into the sarcoplasm, they are immediately bound to Fabp3. This binding also provides a positive feedback for more fatty acid uptake. Bound fatty acids can then be transported intracellularly for β-oxidation in the mitochondria to produce ATPs, for triglyceride synthesis to avoid lipid toxicity from elevated fatty acid concentrations, and for bioactive lipid mediator production to regulate physiological function of the muscle. In *znt7*-KO muscle cells, fatty acid uptake and Fabp3 binding are up-regulated, leading to increased β-oxidation in the mitochondria. However, it seems that the increased β-oxidation cannot keep up with the increased fatty acid levels in the *znt7*-KO muscle cell. Excessive levels of fatty acids are converted into lipids and lipid mediators, resulting in inflammation and oxidative stress, two key processes that drive insulin resistance.

Intraperitoneal insulin tolerance test

Before the test, mice were fasted for 4 h and weighed. Insulin (5.5 units of Humulin® R (U-100)/kg of body weight; Lilly) was given intraperitoneally. Blood glucose was determined at 0, 15, 30, 60, and 120 min after insulin injection using a One-Touch UltraMini meter.

Lipid extraction and analysis

Femoral muscle or liver was pulverized on dry ice, and an aliquot of muscle (75–100 mg) or liver ($\sim$50 mg) was then transferred into 2-ml polypropylene tubes. The subsequent procedures for total lipid extraction were described previously (5, 31). Samples were spiked with analytical surrogates, triglyceride (16:0-d_{31}), cholesteryl ester (22:1(n-9)), free fatty acids (22:3(n-3) and 15:1(n-5)), phosphatidylcholine (18:0-d_{35}), and a suite of deuterated oxylipins. The extracted subsamples were processed and analyzed by GC-MS on an Agilent 6890 Plus+ GC with 5973N MSD using a DB-225ms 30-m column for fatty acids (32) and by LC-MS/MS on a Sciex 4000 QTRAP with an Acquity UPLC BEH C$_{18}$ column (1.7 μm, 2.1 $\times$ 50 mm; Waters Corp.) for oxylipins (32). All reported values were quantified against authentic calibration curves and adjusted for surrogate recoveries. Total fatty acids were calculated by summation of the fatty acids quantified (12:0, 14:0, 16:0, 16:1(n-7), 16:1(n-7)t, 18:0, 18:1(n-7), 18:1(n-9), 18:2 *trans*-10, *cis*-12, 18:2 *cis*-9, *trans*-11, 18:2(n-6), 18:3(n-3), 18:3(n-6), 18:4(n-3), 20:0, 20:1(n-9), 20:2(n-6), 20:3(n-3), 20:3(n-6), 20:4(n-6), 20:5(n-3), 22:0, 22:2(n-6), 22:4(n-6), 22:5(n-3), 22:5(n-6), 22:6(n-3), 24:0, and 24:1(n-9)). Total SFAs were calculated by summation of 12:0, 14:0, 16:0, and 18:0. Total MUFAs were the sum of all fatty acids with one double bond, and total PUFAs were the sum of all fatty acids with two or more double bonds. The ratio of n-6 to n-3 fatty acids was calculated by the sum of n-6 PUFAs divided by the sum of n-3 PUFAs.

Oil Red O staining of skeletal muscle

Femoral skeletal muscle was dissected and rinsed in ice-cold 1$\times$ PBS, blotted dry, and placed in ice-cold 4% paraformalde-hyde overnight at 4 °C. Tissue was washed with 10 ml of 1$\times$ PBS buffer (pH 7.4) for 2, 10, and 30 min; blotted dry; and placed in ice-cold 30% sucrose overnight at 4 °C. Muscle was then embedded in optimal cutting temperature compound (OCT) in a liquid nitrogen–chilled isopentane bath. Muscle was then sectioned in 8-μm thicknesses and allowed to dry overnight at room temperature. Muscle was subsequently stained with Oil Red O and counterstained with Harris modified hematoxylin and Light Green.

Immunohistochemistry

Femoral skeletal muscle and liver were dissected, fixed, paraffin-embedded, and sectioned as described previously (8). Tissues were stained with an antibody against mouse ZnT7 (33), and sections were counterstained with hematoxylin.

Electron microscopy

Muscle samples were fixed using Karnovsky's fixative in 0.1 M sodium phosphate buffer (Sorenson's) (34). A 1-mm³ piece was cut and washed with the same buffer. Dehydration was accomplished using ascending concentrations of acetone, and then the piece was infiltrated and embedded in an epoxy resin mixture. Ultrathin sections were cut with a diamond knife (Diatome, Hatfield, PA) and picked up on copper grids. The sections were stained with uranyl acetate and lead citrate before viewing on a Phillips CM120 Biotwin (Hillsboro, OR). Digital images were taken with a Gatan BioScan model digital camera (Pleasanton, CA).

Isolation and culture of primary myoblasts and myotubes

Myoblast isolation from skeletal muscle of *znt7*-KO mice was conducted as described previously (4). Briefly, myoblasts were maintained in a growth medium consisting of 40% Ham's F-10, 40% DMEM, 20% FBS (bovine fetal serum), 2.5 ng/ml basic fibroblast growth factor (Gemini Bio-Products, West Sacramento, CA), 100 units/ml penicillin G, and 100 μg/ml streptomycin (Thermo Fisher Scientific, Carlsbad, CA). Myoblasts were differentiated into myotubes in 4–6 days in DMEM con-

taining 2% house serum before harvest for quantitative RT-PCR and Western blot analysis.

L6 myoblasts and differentiation

L6 myoblasts were maintained in DMEM (HyClone Laboratories, Logan, UT) with 4.5 g/liter glucose supplement with 10% FBS (EMD Millipore, Temecula, CA), 100 units/ml penicillin, and 100 μg/ml streptomycin (EMD Millipore). For myotube differentiation, 6×10^4 cells were seeded in 12-well plates. When cells reached 70% confluence (2 days), media were changed to MEM-α supplemented with 2% horse serum. Media were then changed every other day for 7–9 days (4).

Oxylipin treatment

12-HETE and 12,13-DiHOME were obtained from Cayman Chemical (Ann Arbor, MI). 12-HETE and 12,13-DiHOME were purged in N_2 gas and dissolved in 50% ethanol. To determine insulin-dependent Akt phosphorylation, L6 myoblasts (6×10^4) were differentiated for 7 days and treated with 2 μM 12-HETE or 2 μM 12,13-DiHOME at 37 °C for 18 h. After the treatment, L6 myotubes were serum-starved for 2 h and stimulated with 100 nM insulin at 37 °C for 7 min. Cells were washed and harvested for Akt phosphorylation assay using Western blot analysis.

2-[³H]Deoxyglucose uptake assay

L6 myoblasts (6×10^4) were seeded in 12-well plates, and differentiation was induced as described previously (4). After 7-day differentiation, cells were starved in MEM-α in the presence of 2% fatty acid–free BSA (Gold Biotechnology, St. Louis, MO). Then 2 μM 12-HETE or 12,13-DiHOME (Cayman Chemical) was added and incubated for 18 h. The cells were washed and preincubated in KRH buffer (4) at 37 °C for 30 min followed by a 15-min incubation in fresh KRH buffer containing 0.33 μM 2-[³H]deoxyglucose (PerkinElmer Life Sciences) and 150 μM D-glucose in the presence of 0 or 100 nM insulin (Sigma-Aldrich). After insulin stimulation, the cells were washed with ice-cold 1× PBS containing 20 mM D-glucose four times and lysed in 300 μl of 0.1 N NaOH. Radioactivity was determined by liquid scintillation counting. Protein concentrations were determined using a BCA protein assay kit (Thermo Fisher Scientific).

ELISA analysis for Ccl2

L6 myotubes were differentiated as described above. After 7-day differentiation, cells were treated with 10 μM 12-HETE or 12,13-DiHOME in MEM-α containing 2% fatty acid–free BSA at 37 °C for 48 h. The culture medium was collected, and cell debris was removed by centrifugation. The supernatant was collected and stored at −80 °C until use. Ccl2 concentration in the culture medium was quantified using a rat Mcp-1 ELISA kit according to the manufacturer's instructions (Thermo Fisher Scientific).

Total RNA isolation, cDNA synthesis, and quantitative RT-PCR analysis

Total RNA was isolated according to the manufacturer's instructions (Thermo Fisher Scientific). Total RNA (1 μg) was converted into cDNA using an iScript cDNA synthesis kit (Bio-Rad). For quantitative RT-PCR analysis, synthesized cDNA was diluted 10-fold with double-distilled water, and 2 μl was used in a SYBR® Green-based PCR using SsoAdvanced™ SYBR Green Supermix (Bio-Rad). Quantitative PCR was performed on a CFX384 Real-Time System (Bio-Rad). Primers were designed using Primer-Blast (https://www.ncbi.nlm.nih.gov/tools/primer-blast/) or adapted from the PrimerBank (https://pga.mgh.harvard.edu/primerbank/index.html).[4] All primers were confirmed with melting curve analysis. Primer sequences are listed in Table S1. Quantitative PCR was run in triplicate, and the average crossing-point value was used for relative expression calculations ($-2^{\Delta\Delta CT}$ method) (35). The expression of the target genes was normalized to the expression of *Actb*.

Antibody

Antibody against ZnT7 was described previously (33). Antibodies against Fabp3 and Actb were purchased from Proteintech (Chicago, IL) and Sigma-Aldrich, respectively. A mouse monoclonal Hadhb antibody (C-6) was purchased from Santa Cruz Biotechnology (sc-271496; Dallas, TX). Horseradish peroxidase–conjugated secondary antibodies were purchased from Cell Signaling Technology.

[1-¹⁴C]Palmitic acid uptake assay

[1-¹⁴C]Palmitic acid (100 μCi/ml; 55 mCi/mmol) was purchased from MP Biomedicals (Solon, OH). Primary myoblasts (WT and *znt7*-KO) (2.5×10^5 cells/well) were plated in 48-well plates and differentiated into myotubes in 4 days in DMEM containing 2% house serum. Myotubes were preincubated with 0.1% (w/v) fatty acid–free BSA in DMEM for 2 h at 37 °C in 5% CO_2. Preincubation medium was replaced with 250 μl of 80 μM [1-¹⁴C]palmitic acid (1.2 μCi), 40 μM fatty acid–free BSA in DMEM and incubated for 0 or 3 min at 37 °C in 5% CO_2. Uptake was stopped by aspiration of uptake buffer and addition of ice-cold stop buffer (0.1% BSA, 0.2 mM phloretin in DMEM) for 2 min on ice. Cells were washed three times with 300 ml of ice-cold DMEM containing 0.1% fatty acid–free BSA. Cells were lysed by addition of 150 μl of lysis buffer (0.1 N NaOH, 0.2% SDS) and incubated for 30 min on ice. Radioactivity was determined by liquid scintillation counting (Tri-Carb 2500 TR liquid scintillation counter, Packard). Protein concentrations were determined using a BCA protein assay kit (Bio-Rad). Results are mean ± S.D. (three independent experiments with three to six replicate).

Western blot analysis

Primary or L6 myotubes were lysed in M-PER buffer (Thermo Fisher Scientific) containing phosphatase and kinase inhibitors as described previously (4). Protein concentrations were determined using a BCA protein assay (Bio-Rad or Thermo Fisher Scientific). Western blots were performed as described previously (5).

---

[4] Please note that the JBC is not responsible for the long-term archiving and maintenance of this site or any other third party-hosted site.

Ⓢ ASBMB

J. Biol. Chem. (2018) 293(20) 7549–7563 **7561**

ROS detection and quantitation

Primary myoblasts (WT and *znt7*-KO) (~20,000/well) were plated in 96-well black wall/clear bottomed microplates and differentiated into myotubes in 4 days in DMEM containing 2% house serum. To detect and quantify ROS accumulation levels in myotubes, we used a Cellular Reactive Oxygen Species Detection Assay kit (orange fluorescence; Abcam, Cambridge, MA). Cells were preincubated in $1\times$ PBS for 15 min at 37 °C in 5% CO_2. Cells were then incubated in ROS orange stain working solution for 60 min in the dark at 37 °C in 5% CO_2. The orange fluorescence was read using a Spectra Max GEMINI XS microplate reader (excitation, 540 nm; emission, 570 nm; Molecular Devices, Sunnyvale, CA). Protein concentrations were determined using a BCA protein assay kit (Thermo Fisher Scientific). Results are mean ± S.E. (three independent experiments with three to six replicates, $n = 12$).

Data and statistical analysis

Results are presented as the mean ± S.E. or mean ± S.D. Student's *t* test was used in comparisons of two genotype groups. Differences were considered to be significant at $p < 0.05$.

References

1. Huang, L., and Tepaamorndech, S. (2013) The SLC30 family of zinc transporters—a review of current understanding of their biological and pathophysiological roles. *Mol. Aspect Med.* **34,** 548–560 CrossRef Medline
2. Jeong, J., and Eide, D. J. (2013) The SLC39 family of zinc transporters. *Mol. Aspects Med.* **34,** 612–619 CrossRef Medline
3. Thirumoorthy, N., Shyam Sunder, A., Manisenthil Kumar, K., Senthil Kumar, M., Ganesh, G., and Chatterjee, M. (2011) A review of metallothionein isoforms and their role in pathophysiology. *World J. Surg. Oncol.* **9,** 54 CrossRef Medline
4. Huang, L., Kirschke, C. P., Lay, Y. A., Levy, L. B., Lamirande, D. E., and Zhang, P. H. (2012) Znt7-null mice are more susceptible to diet-induced glucose intolerance and insulin resistance. *J. Biol. Chem.* **287,** 33883–33896 CrossRef Medline
5. Tepaamorndech, S., Kirschke, C. P., Pedersen, T. L., Keyes, W. R., Newman, J. W., and Huang, L. (2016) Zinc transporter 7 deficiency affects lipid synthesis in adipocytes by inhibiting insulin-dependent Akt activation and glucose uptake. *FEBS J.* **283,** 378–394 CrossRef Medline
6. Huang, L., Yan, M., and Kirschke, C. P. (2010) Over-expression of ZnT7 increases insulin synthesis and secretion in pancreatic β-cells by promoting insulin gene transcription. *Exp. Cell Res.* **316,** 2630–2643 CrossRef Medline
7. Yu, Y. Y., Kirschke, C. P., and Huang, L. (2007) Immunohistochemical analysis of ZnT1, 4, 5, 6, and 7 in the mouse gastrointestinal tract. *J. Histochem. Cytochem.* **55,** 223–234 CrossRef Medline
8. Kirschke, C. P., and Huang, L. (2008) Expression of the ZNT (SLC30) family members in the epithelium of the mouse prostate during sexual maturation. *J. Mol. Histol.* **39,** 359–370 CrossRef Medline
9. Tepaamorndech, S., Huang, L., and Kirschke, C. P. (2011) A null-mutation in the Znt7 gene accelerates prostate tumor formation in a transgenic adenocarcinoma mouse prostate model. *Cancer Lett.* **308,** 33–42 CrossRef Medline
10. Huang, L., Yu, Y. Y., Kirschke, C. P., Gertz, E. R., and Lloyd, K. K. (2007) Znt7 (Slc30a7)-deficient mice display reduced body zinc status and body fat accumulation. *J. Biol. Chem.* **282,** 37053–37063 CrossRef Medline
11. Tepaamorndech, S., Kirschke, C. P., and Huang, L. (2014) Linking cellular zinc status to body weight and fat mass: mapping quantitative trait loci in Znt7 knockout mice. *Mamm. Genome* **25,** 335–353 CrossRef Medline
12. DeFronzo, R. A., and Tripathy, D. (2009) Skeletal muscle insulin resistance is the primary defect in type 2 diabetes. *Diabetes Care* **32,** Suppl. 2, S157–S163 CrossRef Medline
13. Hulver, M. W., Berggren, J. R., Carper, M. J., Miyazaki, M., Ntambi, J. M., Hoffman, E. P., Thyfault, J. P., Stevens, R., Dohm, G. L., Houmard, J. A., and Muoio, D. M. (2005) Elevated stearoyl-CoA desaturase-1 expression in skeletal muscle contributes to abnormal fatty acid partitioning in obese humans. *Cell Metab.* **2,** 251–261 CrossRef Medline
14. Korotkova, M., and Lundberg, I. E. (2014) The skeletal muscle arachidonic acid cascade in health and inflammatory disease. *Nat. Rev. Rheumatol.* **10,** 295–303 CrossRef Medline
15. Calder, P. C. (2010) ω-3 fatty acids and inflammatory processes. *Nutrients* **2,** 355–374 CrossRef Medline
16. Ogata, T., and Yamasaki, Y. (1997) Ultra-high-resolution scanning electron microscopy of mitochondria and sarcoplasmic reticulum arrangement in human red, white, and intermediate muscle fibers. *Anat. Rec.* **248,** 214–223 Medline
17. Gabbs, M., Leng, S., Devassy, J. G., Monirujjaman, M., and Aukema, H. M. (2015) Advances in our understanding of oxylipins derived from dietary PUFAs. *Adv. Nutr.* **6,** 513–540 CrossRef Medline
18. Sell, H., Dietze-Schroeder, D., Kaiser, U., and Eckel, J. (2006) Monocyte chemotactic protein-1 is a potential player in the negative cross-talk between adipose tissue and skeletal muscle. *Endocrinology* **147,** 2458–2467 CrossRef Medline
19. Heilbronn, L., Smith, S. R., and Ravussin, E. (2004) Failure of fat cell proliferation, mitochondrial function and fat oxidation results in ectopic fat storage, insulin resistance and type II diabetes mellitus. *Int. J. Obes. Relat. Metab. Disord.* **28,** Suppl. 4, S12–S21 CrossRef Medline
20. Attie, A. D., Krauss, R. M., Gray-Keller, M. P., Brownlie, A., Miyazaki, M., Kastelein, J. J., Lusis, A. J., Stalenhoef, A. F., Stoehr, J. P., Hayden, M. R., and Ntambi, J. M. (2002) Relationship between stearoyl-CoA desaturase activity and plasma triglycerides in human and mouse hypertriglyceridemia. *J. Lipid Res.* **43,** 1899–1907 CrossRef Medline
21. Jeromson, S., Gallagher, I. J., Galloway, S. D., and Hamilton, D. L. (2015) ω-3 fatty acids and skeletal muscle health. *Mar. Drugs* **13,** 6977–7004 CrossRef Medline
22. Zschiesche, W., Kleine, A. H., Spitzer, E., Veerkamp, J. H., and Glatz, J. F. (1995) Histochemical localization of heart-type fatty-acid binding protein in human and murine tissues. *Histochem. Cell Biol.* **103,** 147–156 CrossRef Medline
23. Glatz, J. F., Schaap, F. G., Binas, B., Bonen, A., van der Vusse, G. J., and Luiken, J. J. (2003) Cytoplasmic fatty acid-binding protein facilitates fatty acid utilization by skeletal muscle. *Acta Physiol. Scand.* **178,** 367–371 CrossRef Medline
24. Kusudo, T., Kontani, Y., Kataoka, N., Ando, F., Shimokata, H., and Yamashita, H. (2011) Fatty acid-binding protein 3 stimulates glucose uptake by facilitating AS160 phosphorylation in mouse muscle cells. *Genes Cells* **16,** 681–691 CrossRef Medline
25. Shearer, J., Fueger, P. T., Bracy, D. P., Wasserman, D. H., and Rottman, J. N. (2005) Partial gene deletion of heart-type fatty acid-binding protein limits the severity of dietary-induced insulin resistance. *Diabetes* **54,** 3133–3139 CrossRef Medline

ASBMB

26. Yamashita, H., Wang, Z., Wang, Y., Segawa, M., Kusudo, T., and Kontani, Y. (2008) Induction of fatty acid-binding protein 3 in brown adipose tissue correlates with increased demand for adaptive thermogenesis in rodents. *Biochem. Biophys. Res. Commun.* **377,** 632– 635 CrossRef Medline

27. Dobrian, A. D., Lieb, D. C., Cole, B. K., Taylor-Fishwick, D. A., Chakrabarti, S. K., and Nadler, J. L. (2011) Functional and pathological roles of the 12- and 15-lipoxygenases. *Prog. Lipid Res.* **50,** 115–131 CrossRef Medline

28. Marinescu, V. D., Kohane, I. S., and Riva, A. (2005) The MAPPER database: a multi-genome catalog of putative transcription factor binding sites. *Nucleic Acids Res.* **33,** D91–D97 CrossRef Medline

29. Standage, S. W., Bennion, B. G., Knowles, T. O., Ledee, D. R., Portman, M. A., McGuire, J. K., Liles, W. C., and Olson, A. K. (2017) PPARα augments heart function and cardiac fatty acid oxidation in early experimental polymicrobial sepsis. *Am. J. Physiol. Heart Circ. Physiol.* **312,** H239 –H249 CrossRef Medline

30. Zhang, J., Phillips, D. I., Wang, C., and Byrne, C. D. (2004) Human skeletal muscle PPARα expression correlates with fat metabolism gene expression but not BMI or insulin sensitivity. *Am. J. Physiol. Endocrinol. Metab.* **286,** E168 –E175 CrossRef Medline

31. Smedes, F., and Askland, T. K. (1999) Revisiting the development of the Bligh and Dyer total lipid determination method. *Mar. Pollut. Bull.* **38,** 193–201 CrossRef

32. Grapov, D., Adams, S. H., Pedersen, T. L., Garvey, W. T., and Newman, J. W. (2012) Type 2 diabetes associated changes in the plasma non-esterified fatty acids, oxylipins and endocannabinoids. *PLoS One* **7,** e48852 CrossRef Medline

33. Kirschke, C. P., and Huang, L. (2003) ZnT7, a novel mammalian zinc transporter, accumulates zinc in the Golgi apparatus. *J. Biol. Chem.* **278,** 4096 – 4102 CrossRef Medline

34. Bozzola J. J., and Russell, L. D. (1992) Specimen preparation for transmission electron microscopy, in *Electron Microscopy: Principles and Techniques for Biologists*, pp. 16 – 47, Jones and Bartlett Publishers, Boston, MA

35. Livak, K. J., and Schmittgen, T. D. (2001) Analysis of relative gene expression data using real-time quantitative PCR and the $2^{-\Delta\Delta CT}$ method. *Methods* **25,** 402– 408 CrossRef Medline